

## RESEARCH ARTICLE

10.1002/2013JD021245

## Key Points:

- Changes in future monthly PET are substantial for HadCM3
- Future PET changes are mainly due to changes in three climatic variables
- Causes of future PET changes are varied at different stations and months

## Correspondence to:

Y.-P. Xu,  
yuepingxu@zju.edu.cn

## Citation:

Xu, Y.-P., S. Pan, G. Fu, Y. Tian, and X. Zhang (2014), Future potential evapotranspiration changes and contribution analysis in Zhejiang Province, East China, *J. Geophys. Res. Atmos.*, 118, 2174–2192, doi:10.1002/2013JD021245.

Received 25 NOV 2013

Accepted 3 FEB 2014

Accepted article online 11 FEB 2014

Published online 11 MAR 2014

## Future potential evapotranspiration changes and contribution analysis in Zhejiang Province, East China

Yue-Ping Xu<sup>1</sup>, Suli Pan<sup>1</sup>, Guangtao Fu<sup>2</sup>, Ye Tian<sup>1</sup>, and Xujie Zhang<sup>1</sup>

<sup>1</sup>Institute of Hydrology and Water Resources, Civil Engineering, Zhejiang University, Hangzhou, China, <sup>2</sup>Centre for Water Systems, College of Engineering, Mathematics and Physical Sciences, University of Exeter, Exeter, UK

**Abstract** Potential evapotranspiration is an important component of hydrological modeling. In this study, the objective is to project potential evapotranspiration in the future period 2011–2040 and understand their changes in Zhejiang Province, East China. The sensitivity of potential evapotranspiration to five climatic variables (solar radiation, daily minimum and maximum air temperature, relative humidity, and wind speed) is analyzed based on observation data from 1955–2008 using a global sensitivity analysis method, Sobol's method. The changes in potential evapotranspiration during the future period are generated using one regional climate model, Providing Regional Climates for Impacts Studies, with two global climate models, ECHAM5 and Hadley Centre Coupled Model version 3, and their causes are analyzed based on sensitivity analysis results. Global sensitivity analysis results reveal substantial spatial-temporal variations in the sensitivity of potential evapotranspiration to climatic variables and unignorable interactions among climatic variables. Rather similar spatial change patterns of annual mean potential evapotranspiration (PET) are generated for both general circulation models; however, seasonal or monthly changes are very different due to different spatial-temporal changes in climatic variables. Different contributory sources to potential evapotranspiration changes are identified at different months and stations; the PET changes in 2011–2040 are mainly due to three climatic variables including solar radiation, relative humidity, and daily minimum temperature.

### 1. Introduction

Evapotranspiration (ET), including evaporation and transpiration, plays a crucial role in the heat and mass fluxes of global and regional atmospheric systems. Understanding the mechanism of ET is vital in agricultural and hydrological studies at both global and regional scales [Liu *et al.*, 2004; McVicar *et al.*, 2007; Gu *et al.*, 2008; Van der Velde *et al.*, 2013]. The most important expressions of ET include potential evapotranspiration (PET), pan evaporation, and actual evapotranspiration; in particular, PET is a central element in hydrological modeling and agricultural water management. Many studies have investigated the spatiotemporal variability of PET in different regions [Xu *et al.*, 2006; McVicar *et al.*, 2007; Li *et al.*, 2012; Fan and Thomas, 2013]. In China, a lot of attention on potential evapotranspiration has also been gained in recent years [Ge *et al.*, 2006; Li and Zhang, 2011; Wang *et al.*, 2011, 2013], which have provided valuable information for diverse sectors such as agriculture, hydrology, and forestry.

However, it is difficult to measure PET directly and many formulations have been therefore developed to estimate potential evapotranspiration. They are generally classified into three categories. The first category is temperature-based formulations, which use temperature as the main input, including the Hargreaves method [Hargreaves and Samni, 1982, 1985] and Blaney-Cridde method [Blaney and Cridde, 1950]. The second category is radiation-based formulations, such as Makkink method [Makkink, 1957] and Priestley-Taylor method [Priestley and Taylor, 1972]. The last category is mass transfer based methods, including Rohwer method [Rohwer, 1931]. The well-known Penman-Monteith (PM) method belongs to a mixture of the last two categories. Many researches focused on the comparison of the above methods such as the work by Xu and Singh [2000, 2001] and indicated that the Penman-Monteith (PM) method is probably the most appropriate method to estimate PET [Diodato and Bellocchi, 2007; Donohue *et al.*, 2010].

Understanding the impact of climate variability/change on hydrological cycles is critical for water management. Changes in precipitation and temperature have been widely investigated [e.g., Fowler *et al.*, 2007; Li *et al.*, 2007; Onof and Arnbjerg-Nielsen, 2009; Xu *et al.*, 2012]. However, the future changes in PET or actual evapotranspiration

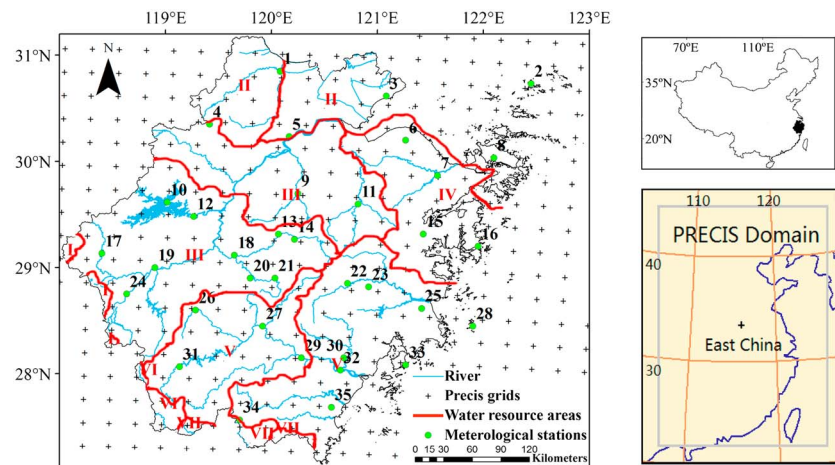


**Figure 1.** Location of Zhejiang Province and meteorological stations used in the study.

due to climate change are less often investigated. *Li et al.* [2012] investigated the spatiotemporal characteristics of PET during 2011–2099 on the Loess Plateau of China and found a continuous increase in PET in the future using Hadley Centre Coupled Model version 3 (HadCM3) and downscaling software SDSM (Statistical Downscaling Model). *Wang et al.* [2013] investigated the future changes in PET across the Tibetan Plateau using SDSM.

In many climate change impact analysis studies on hydrology or water resources, only temperature and precipitation are incorporated into hydrological models by using temperature-based PET estimation methods or just ignoring the changes in other climatic variables [e.g., *Jha et al.*, 2004; *Wang et al.*, 2012; *Xu et al.*, 2013]. *Wang et al.* [2012] used projected daily temperature and precipitation in the future to drive a large-scale hydrological model (Variable Infiltration Capacity model) to assess water resources in China and kept other climatic variables unchanged. However, solar radiation, wind speed, and relative humidity might change under future climate change, which will probably invalidate the use of temperature-based PET equations or assumption of unchanged climatic variables. Therefore, it is of importance to investigate the sensitivity of PET to different climatic variables and the impact of future climate change on PET. Several studies have used local sensitivity analysis methods such as first-order approach or sensitivity coefficients to analyze the contributions of different climatic variables to pan evaporation [*Yang and Yang*, 2012] and PET [*Gong et al.*, 2006]. Local sensitivity analysis is usually carried out by computing partial derivatives of the output functions with respect to the input factors or variables and addresses sensitivity relative to point estimates of factor values [*Saltelli et al.*, 2000]. Using these methods, interactions among different input factors are often ignored. Recently, more complicated sensitivity analysis methods like global sensitivity analysis methods become increasingly used [*Xu and Mynett*, 2006; *Haynes and Millet*, 2013]. A global sensitivity analysis examines sensitivity with regard to the entire factor space, by apportioning the output uncertainty to the uncertainty in the input factors, described by probability distribution functions that cover the factors' range of existence. Global sensitivity analysis has the advantage of considering interactions between concerned input factors and is able to provide more information for contribution analysis.

The aim of this study is therefore threefold: (1) to identify the sensitive climatic variables to PET using a global sensitivity analysis method, Sobol's method, in Zhejiang Province, East China; (2) to project future changes in PET in the period 2011–2040 using a regional climate model, Providing Regional Climates for Impacts Studies (PRECIS); (3) to analyze the contributions of different climatic variables to PET changes in the future period. In the analysis, the climatic variables include daily minimum and maximum air temperature, solar radiation, wind speed, and relative humidity.

## 2. Materials and Methods

### 2.1. Study Area

Zhejiang Province (118°E–123°E, 27°N–31°N), with an area of about  $1.04 \times 10^5$  km<sup>2</sup>, is located in East China, Asia (see Figure 1). The dominant climate of the province is Asian subtropical monsoon, which is characterized by abundant precipitation and high temperature in summer and dry and cold winters. The annual mean temperature

**Table 1.** Meteorological Stations Used in This Study

No.	Station Name	Period	No.	Station Name	Period
1	Huzhou	1961–2012	19	Quzhou	1956–2008
2	Shengsi	1959–2008	20	Wuyi	1962–2011
3	Pinghu	1955–2008	21	Yongkang	1962–2011
4	Tianmushan	1956–1998	22	Xianju	1961–2012
5	Hangzhou	1954–2011	23	Kuocangshan	1956–1993
6	Cixi	1954–2008	24	Jiangshan	1961–2012
7	Yinxian	1954–2008	25	Hongjia	1955–2008
8	Dinghai	1955–2008	26	Suichang	1961–2012
9	Zhuji	1970–2012	27	Lishui	1955–2008
10	Chunan	1971–2004	28	Dachendao	1959–2008
11	Shengxian	1957–2008	29	Qingtian	1971–2012
12	Jiande	1971–2004	30	Yongjia	1971–2012
13	Yiwu	1962–2011	31	Longquan	1954–2008
14	Dongyang	1962–2011	32	Wenzhou	1952–2000
15	Ninghai	1961–2012	33	Yuhuan	1957–2008
16	Shipu	1956–2008	34	Taishun	1961–2012
17	Kaihua	1961–2012	35	Pingyang	1961–2012
18	Jinhua	1954–2008			

is 15°C–18°C. The annual mean precipitation varies between 980 and 2000 mm. Mountains and hills dominate the province. Due to the uneven temporal distribution of precipitation, Zhejiang Province suffers a lot from floods, droughts, and typhoons. In this province, there are eight river basins: Qiantang, Ou, Lin, Tiaoxi, Yong, Feiyun, and Ao river basins and the well-known Beijing-Hangzhou canal.

## 2.2. Data

The data used in this study are collected from 35 meteorological stations operated by Zhejiang Meteorological Administration (see Table 1). The majority of the stations have a complete record of several climatic variables from 1955 to 2008. The main climatic variables include maximum and minimum air temperatures at 2 m height, wind speed at 10 m height, precipitation, relative humidity, and sunshine duration at a daily time step.

According to *Zhejiang Provincial Hydrology Bureau* [2005], the whole province is divided into seven water resource areas, i.e., Boyanghu river systems, Taihu river systems, Qiantang river systems, Eastern Zhejiang river systems, Southern Zhejiang river systems, Mingjiang river systems, and East Ming river systems (see Figure 1). The PET will be analyzed based on this division but only concern four water resource areas since the other three water resource areas are very small and no meteorological data are obtained. Table 2 shows the seven water resource areas and their representative stations which will be used later for sensitivity analysis. The representative stations are chosen based on their geographical locations and meteorological conditions.

## 2.3. Methodology

### 2.3.1. Regional Climate Model

The regional climate model PRECIS (Providing Regional Climates for Impacts Studies, <http://www.metoffice.gov.uk/precis/>) is used to downscale meteorological data from global climate models. This regional climate model was developed by the MetOffice Hadley Centre, UK, and can be used to generate detailed climate change projections in any area of the globe [Jones et al., 2004]. Zhang et al. [2006] applied the PRECIS model to simulate the distribution of extreme climate events in China in both the baseline period (1961–1990) and a future period (2071–2100) under the B2 scenario. The results show that PRECIS simulated the spatial distribution

**Table 2.** Water Resource Areas and Their Representative Stations

Divisions	Seven Water Resource Areas	Representative Meteorological Stations	Areas (km <sup>2</sup> )
I	Boyanghu river systems	None	511.1
II	Taihu river systems	Hangzhou	12,273.5
III	Qiantang river systems	Cunan (upstream), Tianmushan (downstream)	42,266.6
IV	Eastern Zhejiang river systems	Dinghai	12,872.2
V	Southern Zhejiang river systems	Lishui (inland), Dachendao (islands)	33,495.2
VI	Mingjiang river systems	None	1,129.8
VII	East Ming river systems	None	1,237

of extreme climate events very well in the baseline period compared with observations. Therefore, this regional climate model is chosen in this study.

Mainly limited by the data provided by MetOffice Hadley Centre, UK, only outputs from two global climate models are used as boundary data for the regional climate model. Although such choice is rather limited, it can still fulfill the purpose of this study. One global climate model used in this study is ECHAM5, which is the fifth-generation atmospheric general circulation model developed at the Max Planck Institute for Meteorology [Simmons *et al.*, 1989]. The ECHAM5 core is composed of a dynamical part, formulated in spherical harmonics and evaluated at a set of almost regularly distributed grid points (the Gaussian grid). The atmospheric model resolution is about  $2.8 \times 2.8^\circ$  latitude-longitude [Roeckner *et al.*, 2003]. The second climate model used in this study is HadCM3, standing for the Hadley Centre Coupled Model version 3. This model is one of the main models used in the Intergovernmental Panel on Climate Change Third and Fourth Assessments and is a coupled atmosphere-ocean general circulation model (GCM) developed at the Hadley Centre [Gordon *et al.*, 2000; Reichler and Kim, 2008]. Its atmospheric component has 19 levels with a horizontal resolution of  $2.5^\circ$  latitude by  $3.75^\circ$  longitude, which produces a global grid of  $96 \times 73$  grid cells. This model has the capability of capturing the time-dependent fingerprint of historical climate change in response to natural and anthropogenic forcing [Stott *et al.*, 2000].

Xu *et al.* [2007] compared the statistic features of 20 year mean simulation and observation in East Asia during 1980–1999 and found out that HadCM3 performs better than ECHAM5 in simulating temperature and precipitation in East Asia. Heo *et al.* [2013] also found that ECHAM5 projects higher temperature than HadCM3 in East Asia.

The simulation domain in this study is the whole East China, mainly including Zhejiang Province (see Figure 1). This simulation is different from all the other PRECIS-related studies in China [Xu *et al.*, 2005; Wang *et al.*, 2012; Tian *et al.*, 2013], which have used future PRECIS outputs run by the Institute of Environment and Sustainable Development in Agriculture, Chinese Academy of Agricultural Sciences, using the whole of China as the domain with a spatial resolution of 50 km. The central point of the simulation in this study is located at  $116^\circ\text{E}$  and  $33.5^\circ\text{N}$ . The resolution of PRECIS outputs is 25 km. The emission scenario used in this study is A1B, which describes a future world of very rapid economic growth, a global population that peaks in midcentury and declines thereafter, and rapid introduction of new and more efficient technologies but with balanced energy sources. The PRECIS grids covering the study area are shown in Figure 1.

### 2.3.2. Penman-Monteith Method and Delta Change Method

The Penman-Monteith method is believed to be able to estimate potential evapotranspiration (PET) more realistically than other methods [Donohue *et al.*, 2010]. Therefore, in this study, the Food and Agriculture Organization of the United Nations (FAO) Penman-Monteith method (PM) method [Allen *et al.*, 1994] is used to estimate the PET in Zhejiang Province. The formula for the FAO-PM method is

$$ET = \frac{0.408\Delta(R_n - G) + \gamma \frac{900}{T_a + 273} u_2 (e_s - e_a)}{\Delta + \gamma(1 + 0.34u_2)} \quad (1)$$

where ET is potential evapotranspiration ( $\text{mm d}^{-1}$ );  $R_n$  is net radiation at the crop surface ( $\text{MJ m}^{-2} \text{d}^{-1}$ );  $G$  is soil heat flux density at the soil surface ( $\text{MJ m}^{-2} \text{d}^{-1}$ );  $T$  is mean daily air temperature at 2 m height ( $^\circ\text{C}$ );  $u_2$  is wind speed at 2 m height (m/s);  $e_s$  is saturation vapor pressure at 2 m height (kPa);  $e_a$  is actual vapor pressure at 2 m height (kPa);  $\Delta$  is slope of the vapor pressure-temperature curve ( $\text{kPa}/^\circ\text{C}$ ); and  $\gamma$  is psychrometric constant ( $\text{kPa}/^\circ\text{C}$ ).

A Delta change method is used to obtain future potential evapotranspiration projections by adding changes in the PET in the future period (2011–2040) to the PET in the baseline period. It is a direct and simple way of avoiding the possible effects of bias in the climatic variables derived from the regional climate model on PET projections. The formulas are as follows:

$$PET_{\text{future}} = PET_{\text{changes}} + PET_{\text{observation}} \quad (2)$$

$$PET_{\text{changes}} = PET_{\text{PRECIS-future}} - PET_{\text{PRECIS-baseline}} \quad (3)$$

where  $PET_{\text{observation}}$  is potential evapotranspiration calculated based on observed climatic variables (mm);  $PET_{\text{PRECIS-future}}$  is potential evapotranspiration calculated based on PRECIS simulations with two GCMs as boundary data in the future period (mm); and  $PET_{\text{PRECIS-baseline}}$  is potential evapotranspiration calculated based on PRECIS simulations in the baseline period (mm).

### 2.3.3. Sobol's Sensitivity Analysis Method

Sobol's sensitivity analysis method [Sobol, 1993; Saltelli et al., 2000], a variance-based method, is chosen here for global sensitivity analysis since this method is superior to traditional sensitivity analysis methods when considering nonlinearity and is robust [Saltelli and Annoni, 2010; Yang, 2011; Zhang et al., 2013]. It has the capability of describing how individual variables and their interactions impact model performance. Interactions occur when the perturbation of two or more variables simultaneously causes variation in the output greater than that of varying each of the variables alone. Such interactions are present in any model that is nonadditive but will be neglected by local sensitivity analysis methods. In Sobol's method, the variance of the model outputs is decomposed into different components that result from individual variables and interactions among variables.

The main idea behind Sobol's method is to decompose the function  $f(\mathbf{x})$  into summands of increasing dimensionality

$$f(x_1, \dots, x_k) = f_0 + \sum_{i=1}^k f_i(x_i) + \sum_{1 \leq i < j \leq k} f_{ij}(x_i, x_j) + \dots + f_{1,2,\dots,k}(x_1, \dots, x_k) \quad (4)$$

For this equation to hold,  $f_0$  must be a constant and the integrals of every summand over any of its own variables must be zero. With this, it is known that all the summands in equation (4) are orthogonal. This means that if  $(i_1, \dots, i_s) \neq (j_1, \dots, j_s)$ , then

$$\int_0^1 f_{i_1, \dots, i_s}(x_{i_1}, \dots, x_{i_s}) dx_{i_k} = 0 \quad \text{if } 1 \leq k \leq s \quad (5)$$

The total variance  $D$  of  $f(x)$  is defined as

$$D = \int_{\Omega^k} f^2(x) dx - f_0^2 \quad (6)$$

While partial variances can be computed from equation (4)

$$D_{i_1, \dots, i_s} = \int_0^1 \dots \int_0^1 f_{i_1, \dots, i_s}^2(x_{i_1}, \dots, x_{i_s}) dx_{i_1} \dots dx_{i_s} \quad (7)$$

where  $1 \leq i_1 < \dots < i_s \leq k$  and  $s = 1, \dots, k$ . Squaring and integrating equations (4) and (5), the total variance  $D$  becomes

$$D = \sum_{i=1}^k D_i + \sum_{1 \leq i < j \leq k} D_{ij} + \dots + D_{1,2,\dots,k} \quad (8)$$

The sensitivity measures are given by

$$S_{i_1, \dots, i_s} = \frac{D_{i_1, \dots, i_s}}{D} \quad \text{for } 1 \leq i_1 < \dots < i_s \leq k \quad (9)$$

Therefore, the sensitivity indices of different orders are as follows

$$\text{First-order effect index } S_i = \frac{D_i}{D} \quad (10)$$

$$\text{Second-order effect index } S_{ij} = \frac{D_{ij}}{D} \quad (11)$$

$$\text{Total effect index } TS(i) = 1 - \frac{D_{-i}}{D} \quad (12)$$

where the first-order effect index  $S_i$  denotes the sensitivity resulting from the main effect of individual parameter  $\theta_i$ ; the second-order effect index  $S_{ij}$  indicates the sensitivity resulting from the interaction of two parameters  $\theta_i$  and  $\theta_j$ ; the total effect sensitivity index represents the main effect of  $\theta_i$  as well as its interactions up to  $k$ th order of analysis; and  $D_{-i}$  indicates the variance resulting from all of the parameters except for  $\theta_i$ .

The variances shown in the above equations can be evaluated by approximate Monte Carlo numerical integrations. The convergence of Monte Carlo integrations is heavily affected by the sampling scheme. Here the quasi-random sequence sampling is used since it samples points more uniformly along the Cartesian grids than uncorrelated random sampling [Tang et al., 2007]. The details of Monte Carlo approximations can be found in Tang et al. [2007] and Fu et al. [2012].

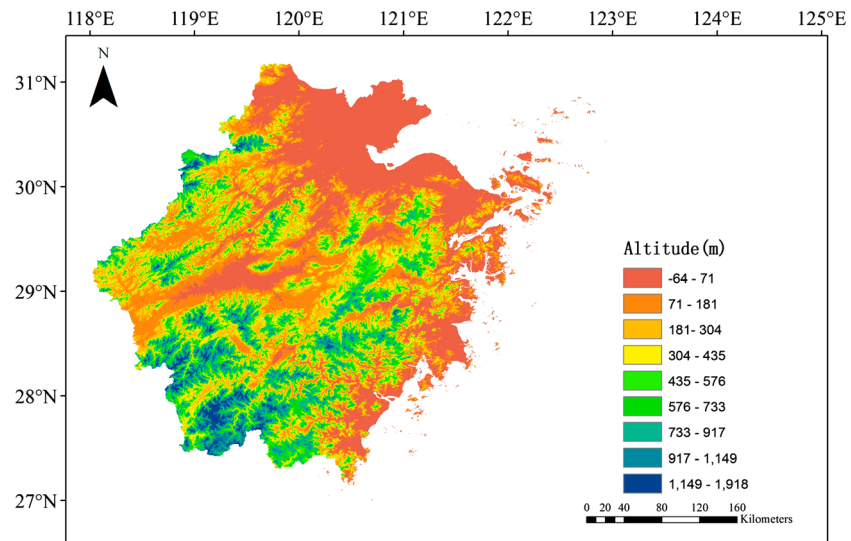


Figure 2. Digital elevation map of the study area.

In this study, the FAO-PM method requires daily minimum and maximum air temperatures, relative humidity, solar radiation, and wind speed as inputs. Since daily maximum and minimum air temperatures are often correlated, average air temperature and daily amplitudes are calculated before obtaining the two random data sets required for Sobol’s sensitivity analysis method (see equations (13) and (14)).

$$T_{\text{mean}} = \frac{T_{\text{max}} + T_{\text{min}}}{2} \tag{13}$$

$$\Delta T = T_{\text{max}} - T_{\text{min}} \tag{14}$$

where  $T_{\text{mean}}$  is daily average air temperature (°C);  $T_{\text{max}}$  is daily maximum air temperature (°C);  $T_{\text{min}}$  is daily minimum air temperature (°C); and  $\Delta T$  is daily air temperature amplitude (°C).

The results of sensitivity analysis will be used further to explain the possible causes of changes in PET in the period 2011–2040 through assuming that the sensitivities of PET to various climatic variables are the same in the baseline period (based on observations) and the future period. Such assumption is made mainly based on the fact that the future climate projections from global climate models or regional climate models are quite uncertain [Kay et al., 2009; Woldemeskel et al., 2012], and therefore it is regarded that the sensitivity of PET to climatic variables based on the future climate model projection is unreliable.

### 2.3.4. Spatial Interpolation

The spatial interpolation is implemented in ArcGIS software based on the digital elevation data downloaded from the Shuttle Radar Topography Mission (SRTM) website (<http://srtm.csi.cgiar.org/>) with a resolution of 90 m by 90 m. Figure 2 shows the digital elevation model of the study area. Considering the possible impact of terrain on the interpolation, the ordinary cokriging approach is used to interpolate the annual, seasonal, and monthly PET in both baseline and future periods. This approach can use elevation as secondary information in interpolation [Goovaerts, 2000]. All 35 meteorological stations are used to obtain spatial information of PET in the study area.

## 3. Results and Analysis

### 3.1. Sensitivity Analysis Results

Only sensitivity analysis results from six representative stations shown in Table 2 are illustrated in this section. The sensitivity analysis is made based on decades of historical observations (1955–2008) for 12 different months. The contribution of different climatic variables to PET output uncertainty is then analyzed on a daily scale for each month at each station.

Figure 3 shows both the first-order and second-order effect sensitivity indices for six representative stations in Zhejiang Province. From this figure, it can be observed that the sensitivity of PET to different climatic variables

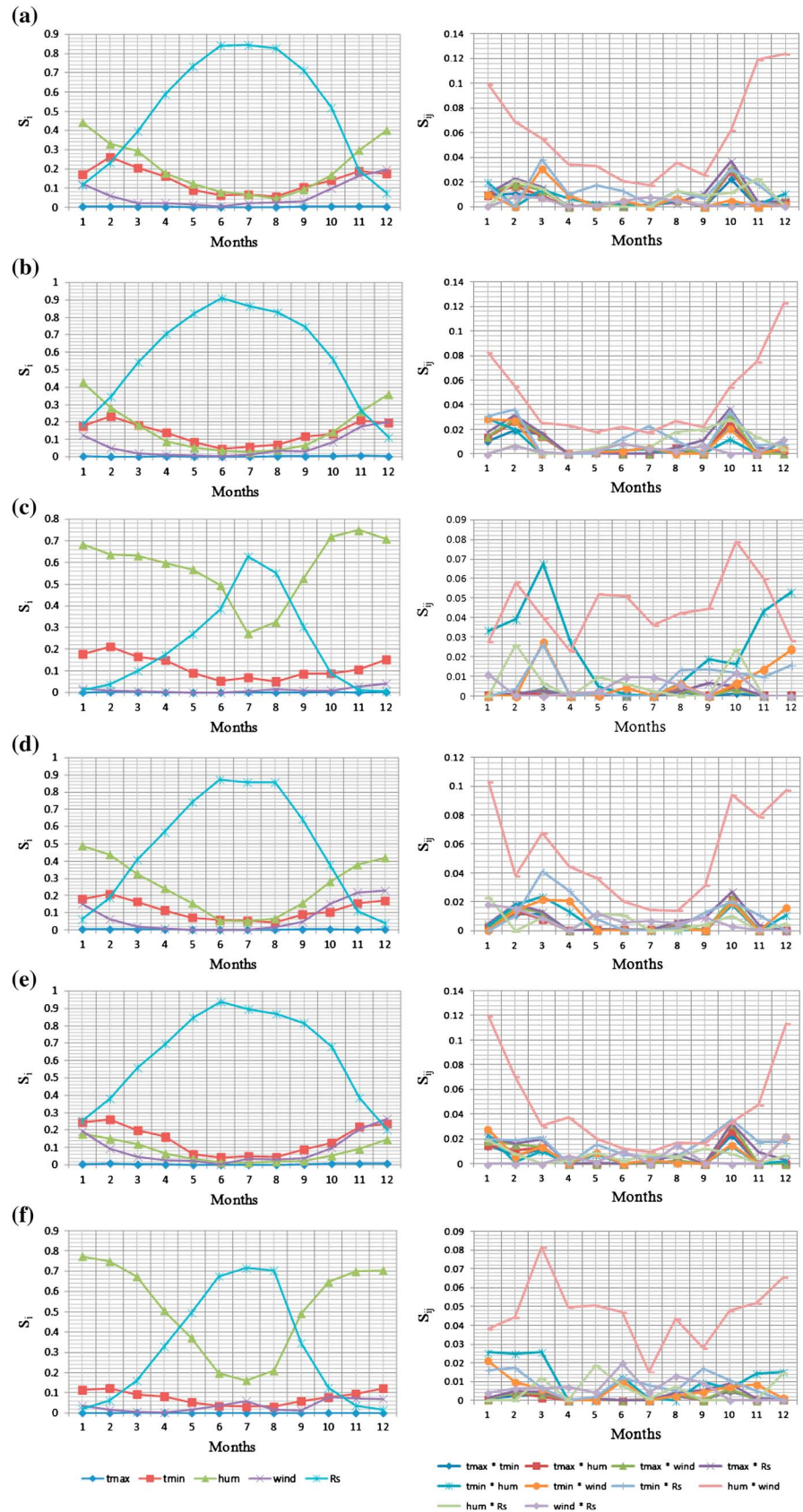
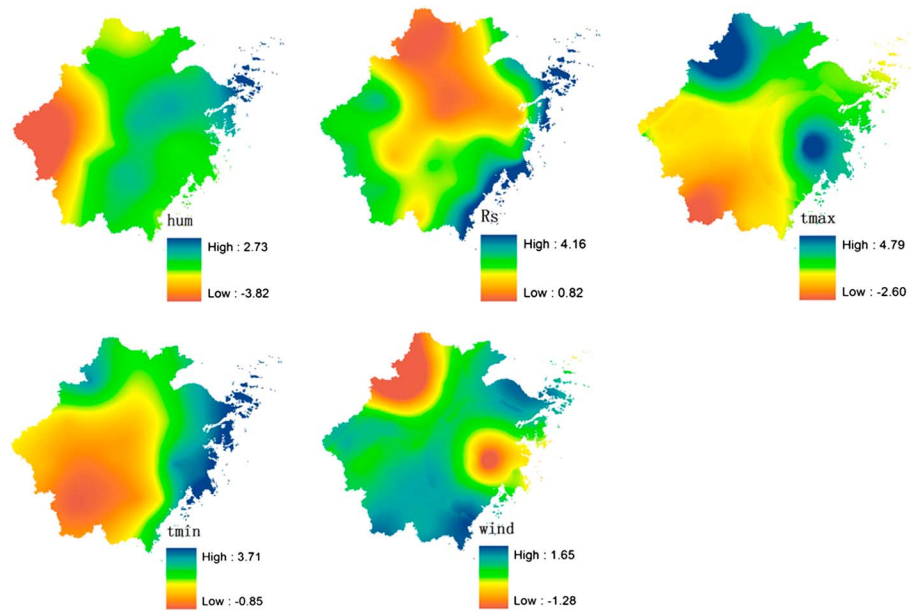


Figure 3



**Figure 4.** Spatial variability of differences of PRECIS-simulated annual mean values of climatic variables and observations. tmax indicates maximum air temperature; tmin represents minimum air temperature; hum represents relative humidity; wind represents wind speed; and Rs is solar radiation.

varies substantially as represented by the first-order effect sensitivity index. In spring, except at Dachendao, Lishui, and Tianmushan, the PET is most sensitive to solar radiation, followed by relative humidity, minimum air temperature, wind speed, and maximum air temperature. In summer, the solar radiation is clearly the dominating climatic variable at all stations. In autumn, the order of sensitivity is similar to that in summer. In winter, however, relative humidity becomes the main source of variation in PET values at all stations except Lishui.

Figure 3 also shows that the PET sensitivity is different at various stations. At Dachendao and Tianmushan, except in summer, relative humidity is the most sensitive variable. Dachendao is located on an island, where its climatic condition is very humid, while Tianmushan is located in the northwest of the province where the elevation is rather high. At Lishui, solar radiation is the dominating climatic factor all through the year except in winter. Different from all the other stations, the daily minimum temperature becomes the second important climatic variable.

The second-order effect sensitivity index shown in Figure 3 reveals the impact of the interactions between climatic variables on the PET variances. For Sobol's sensitivity analysis method, variables or inputs are classified as highly sensitive if they contribute more than 10% variance to the overall PET variance and are classified as sensitive parameters if they contribute more than 1% to the overall PET variance [Tang et al., 2007]. At stations Hangzhou, Cunan, and Lishui, the second-order effect sensitivity index  $S_{ij}$  in winter is up to or more than 0.12 (12%), indicating that PET is highly sensitive to the interactions between wind speed and relative humidity. At Dinghai, PET in winter is also highly sensitive to the interactions between wind speed and relative humidity ( $S_{ij}$  is up to or more than 10%). At stations Tianmushan and Dachendao, PET is sensitive to the interactions between relative humidity and wind speed all the year round. Therefore, considering the interactions, the contribution of wind speed to the variance of PET becomes larger. At Tianmushan, PET is also sensitive to the interactions between relative humidity and daily minimum temperature, ranking the second after the interactions between wind speed and relative humidity. Other interactions cannot be neglected as well since in some months the values of second-order effect sensitivity index are more than 1%. One such example is the interactions between wind speed and daily minimum temperature in March at Hangzhou Station. The second-order sensitivity index

**Figure 3.** (left column) First-order and (right column) second-order effect sensitivity indices calculated at (a) Hangzhou, (b) Cunan, (c) Tianmushan, (d) Dinghai, (e) Lishui, and (f) Dachendao. tmax indicates maximum air temperature; tmin represents minimum air temperature; hum represents relative humidity; wind represents wind speed; Rs is solar radiation; and asterisk indicates second-order effect.

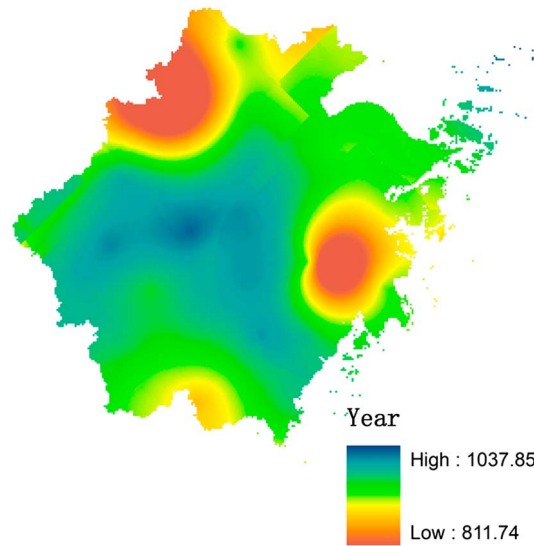


**Figure 5.** Spatial distribution of annual mean PET calculated based on observed climatic variables in the baseline period (mm).

is more than 3%. This indicates that the variances caused by the interactions between wind speed and daily minimum temperature in March contribute more than 3% to the total variances in PET.

Considering the second-order or even higher-order interactions, the contributions of some climatic variables to the overall PET variance become larger. For example, at Dachendao, wind speed is less important than daily minimum temperature in most months in terms of its individual effect on PET. When its interactions with other variables are considered, however, wind speed becomes more important than daily minimum temperature in most months. At Lishui, wind speed becomes the most important climatic variable in winter.

**3.2. Evaluation of PRECIS in the Study Area**

In this section, the performance of PRECIS is briefly evaluated based on the climatic variables used to calculate PET.

Figure 4 shows the spatial variability of differences of PRECIS-simulated annual mean values of five climatic variables and observations in Zhejiang Province. The differences are calculated for individual stations and then interpolated using the cokriging method. It can be figured out that the differences between simulated and observed variables are the smallest for relative humidity, followed by daily maximum temperature, solar radiation, and daily minimum temperature. The wind speed has the largest error. Except wind speed, all other climatic variables are reasonably simulated by the regional climate model in terms of annual mean values.

Correlation coefficients of observed variables and PRECIS-simulated variables on a monthly scale are calculated and compared. The simulated maximum and minimum temperatures show good consistency with the observations. The correlation coefficients of maximum temperatures vary from 0.94 in the west to 0.96 in the coast. The correlation coefficients of minimum temperatures vary from 0.94 in the southwest to 0.97 in the north and coast. Most of the calculated correlation coefficients for solar radiation are above 0.71, with the highest correlation coefficient reaching 0.82. Among all climatic variables, the relative humidity and wind speed, however, have much smaller values of correlation coefficients, indicating that the regional climate model is less capable of simulating these two variables. The highest correlation coefficient of relative humidity is 0.71 (ranging from 0.01 to 0.71), and that of wind speed is 0.73 (ranging from 0.01 to 0.73).

The evaluation results indicate that daily temperature can be modeled by the regional climate model quite well. Solar radiation can be reasonably simulated. However, the other climatic variables including relative humidity and wind speed are less well simulated by the regional climate model, although relative humidity on the annual scale is reasonably simulated. A simple and commonly used approach, Delta change method, is therefore used to obtain future potential evapotranspiration projections by adding changes in the PET in the

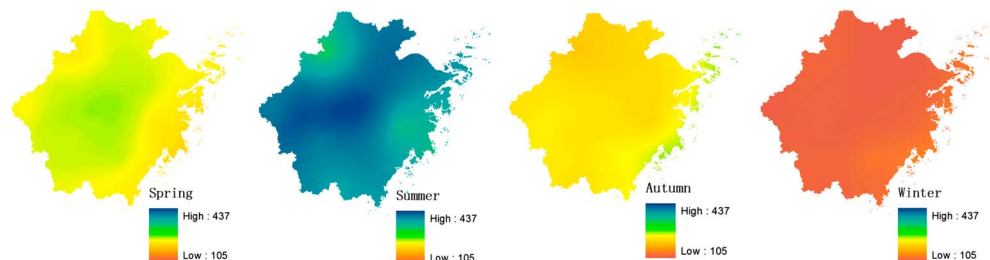


**Figure 6.** Spatial distribution of seasonal PET calculated based on observed climatic variables in the baseline period (mm).

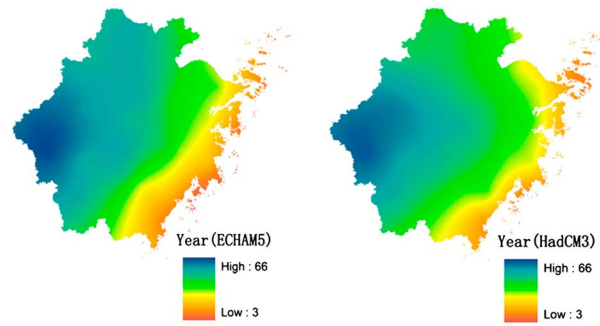


**Figure 7.** Changes of annual mean PET in the future period for two GCMs (mm).

the province. There are two troughs where the annual PET is about 800 mm. One is located in the east of the province (coastal areas), and the other is located in the north of the province.

Figure 6 shows the spatial distribution of seasonal PET calculated based on observed climatic variables in Zhejiang Province in 1961–1990. In spring, the absolute value of PET is relatively small. The value of PET reaches a peak in the center of the province and then reduces to the surroundings. Coastal areas have the lowest PET values. In the northwestern part of the province, low PET can be found as well. In summer, the spatial distribution of PET is rather similar to that in spring. However, due to high solar radiation, the absolute value of PET is the highest in four seasons. In autumn, a rather different pattern from those in spring and summer can be observed. The northern part of the province has the lowest PET, while the coastal area has the highest PET. In winter, most parts of the province have low values of PET. The coastal area again has the highest PET. In winter, the PET has the lowest values in the whole year.

**3.4. Potential Evapotranspiration in the Future Period 2011–2040**

Figure 7 shows the changes in annual mean PET in the future period for two GCMs. Both GCMs show increases in PET in the whole province. The spatial patterns of both changes for two GCMs are similar, with a decreasing trend of changes from the west to the east. The largest change is around 65 mm occurring in the east of the province for ECHAM5, and the smallest increase is around 3 mm, occurring near the coast.

Figure 8 shows the spatial distribution of annual mean PET values for two GCMs and their differences (ECHAM5 minus HadCM3) in the future period. The figure shows that the spatial distribution of future annual mean PET is similar to that in the baseline period. However, for both GCMs, annual mean PET increases in the whole province, although the change percentage is not very large (<10%). It can be observed that ECHAM5 projects larger PET in the north of the province but smaller PET in the coast, although the differences are relatively small.

Figure 9 shows the changes in seasonal PET in the future period for ECHAM5. Except in summer, all the other seasons experience positive changes of PET. In spring, summer, and winter, the positive changes decrease

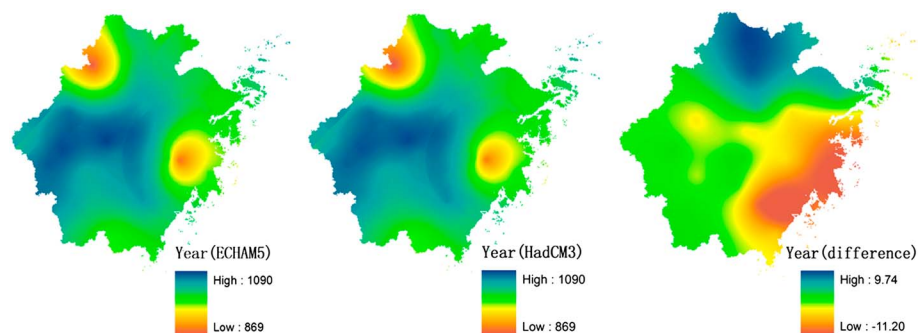


**Figure 8.** Spatial distribution of annual mean PET in the future period for two GCMs and their differences (ECHAM5 minus HadCM3) (mm).

future period (2011–2040) to the PET in the baseline period. By using such method, the effects of bias in all climatic variables from the regional climate model can be avoided on future PET projections.

**3.3. Potential Evapotranspiration in the Baseline Period 1961–1990**

Figure 5 shows the spatial distribution of annual mean PET calculated based on observed climatic variables in Zhejiang Province in 1961–1990. It can be found that the highest PET is located in the center of

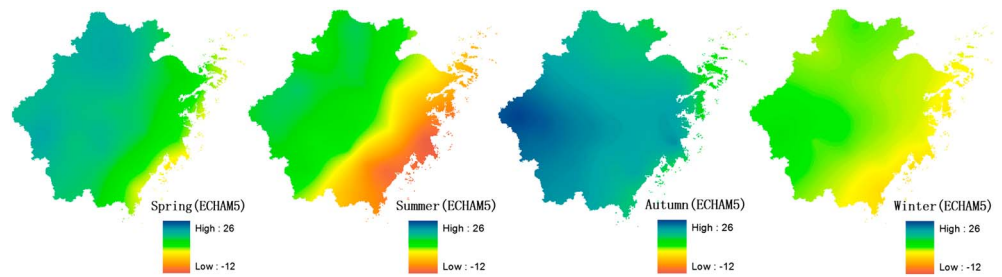


**Figure 9.** Changes in seasonal PET in the future period for ECHAM5 (mm).

from the west to the east. The changes in the PET are the smallest at the coastal regions. In summer, coastal areas experience decrease in PET. In autumn, the northern part of the province experiences the smallest positive changes.

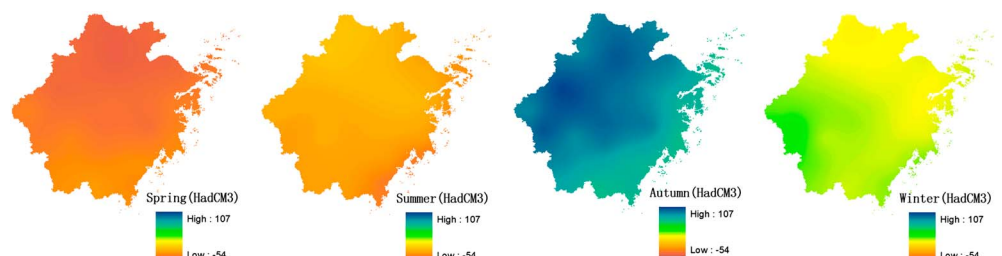
Figure 10 shows the changes in seasonal PET in the future period for HadCM3. The change patterns in the four seasons are very different from those for ECHAM5. In spring and summer, decreases in seasonal PET can be found. In spring, such negative changes increase from the south to north. In summer, the trend is contrary. In autumn and winter, positive changes can be found in the whole province. Such changes decrease from the west to the eastern coastal areas in autumn, while in winter such changes decrease from the southwest to the northeast. The largest increase occurs in autumn, and the largest decrease occurs in spring.

Figure 11 shows the differences of seasonal PET between two GCMs (ECHAM5 minus HadCM3) in the future period. It is found that in spring and summer, ECAHM5 projects larger PET than HadCM3, while in autumn and winter ECAHM5 projects smaller PET. In spring and autumn, the differences between two GCMs are substantial, reaching 72 mm and  $-86$  mm, respectively. This indicates that larger uncertainties exist in future PET projections using different GCMs.

Figure 12 shows the relative changes in monthly PET in the future period at Hangzhou, Dachendao, and Tianmushan, representing the most important water resource areas in the province, i.e., Taihu river systems, Southern Zhejiang river systems, and Qiantang river systems (downstream), respectively. This figure shows that the change patterns at these three stations are rather similar. From February to July, decreases in PET can be observed, while in other months, increases in PET can be found. However, the variations at Tianmushan are the largest, followed by those in Hangzhou and finally those in Dachendao. The change percentages at Hangzhou, Dachendao, and Tianmushan Stations for ECHAM5 range 0.2%~13%,  $-4\%$ ~ $5\%$ , and  $-0.8\%$ ~ $15\%$ , respectively. The change percentages for HadCM3 range  $-26\%$ ~ $59\%$ ,  $-17\%$ ~ $37\%$ , and  $-25\%$ ~ $67\%$ , respectively. ECHAM5 projects even monthly changes but consistently increased PET, while HadCM3 projects decreases from February until July and increases from August until January. Compared to ECHAM5, HadCM3 projects more variations in monthly PET.

**3.5. Causes of Future Changes in Potential Evapotranspiration**

To analyze the causes of PET changes in the future period or link changes in climate variables to PET in the future, Figures 13–15 show the monthly changes of different climatic variables for both GCMs at three representative stations, namely, Hangzhou, Dachendao, and Tianmushan. As stated in section 2.3.3, it is



**Figure 10.** Changes in seasonal PET in the future period for HadCM3 (mm).

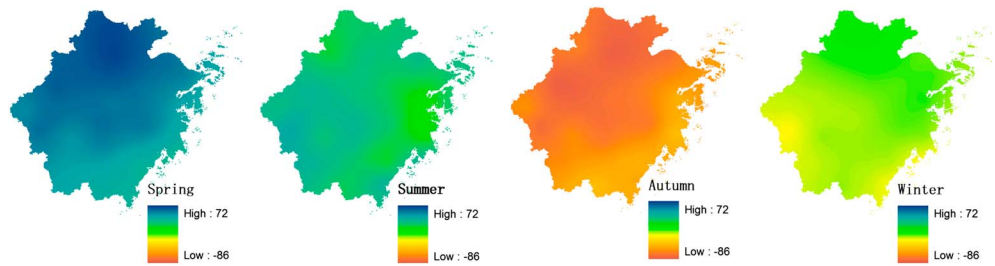


**Figure 11.** Differences of seasonal PET in the future period between two GCMs (ECHAM5 minus HadCM3, mm).

assumed in the following analysis that the sensitivity of PET to different climatic variables in the future period is the same as that in the observation period (shown in Figure 3).

Since the changes for ECHAM5 are insignificant compared to those for HadCM3, the causes of PET changes are mainly analyzed for HadCM3. Figure 12 shows that the decreases for HadCM3 at Hangzhou occur from February to July, in particular April where a relative change reaches  $-26\%$ .

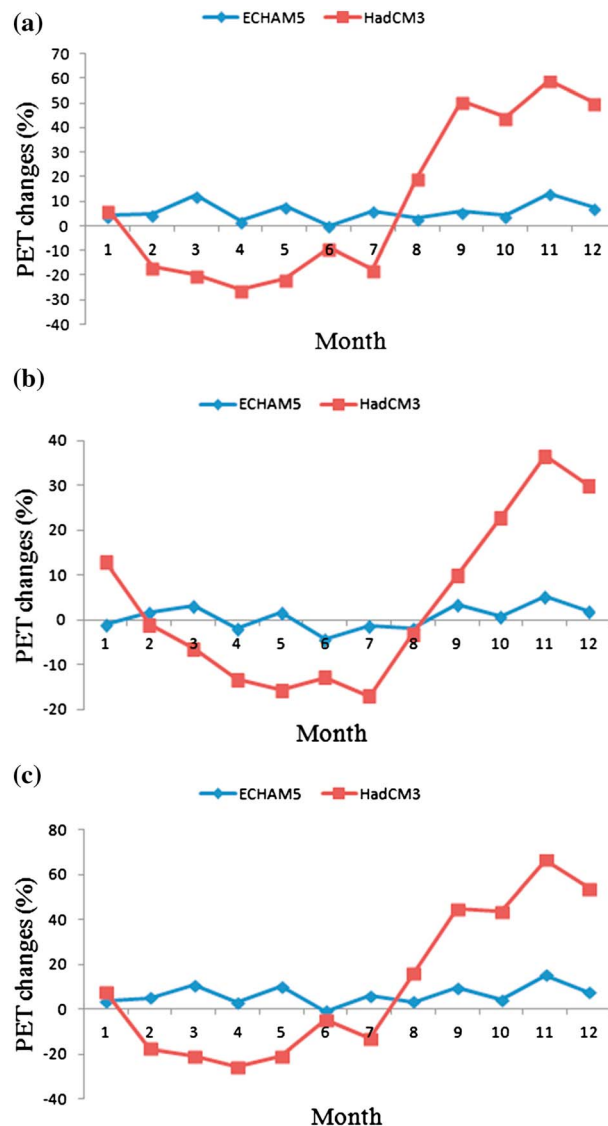


**Figure 12.** Relative changes in monthly PET in the future period at (a) Hangzhou Station, (b) Dachendao Station, and (c) Tianmushan Station.

February to July, in particular April where a relative change reaches  $-26\%$ . According to the sensitivity analysis results shown in Figure 3a, PET in these months at Hangzhou is most sensitive to solar radiation, followed by relative humidity, daily minimum temperature, and wind speed. The role of daily maximum temperature is insignificant. The importance of wind speed is indicated by its interactions with relative humidity. The contributions of wind speed and relative humidity interactions to the total PET variance range from 2% to 7% during this period. Combined with changes shown in Figure 13, it can be figured out that although the role of relative humidity during this period is unclear (see Figure 13b), the decreases in solar radiation and daily minimum temperature are the two main driving forces of PET changes. Take April as an example. The decreases in PET for HadCM3 are the results of combined effects of decrease in solar radiation ( $-28\%$ ) and decrease in daily minimum temperature ( $-27\%$ ). The roles of relative humidity ( $-1\%$ ) and wind speed ( $-0.3\%$ ) are less important.

More importantly, from the sensitivity analysis results, the contributions of climatic variables to PET changes at different stations and months can be revealed and quantified. Take November as an example. The largest increase, 59%, at Hangzhou Station occurs in this month. It is shown in Figure 13 that although relative humidity shows slightly decreasing trend ( $-1.9\%$ ), the changes in other climatic factors are all substantial. The changes in solar radiation,

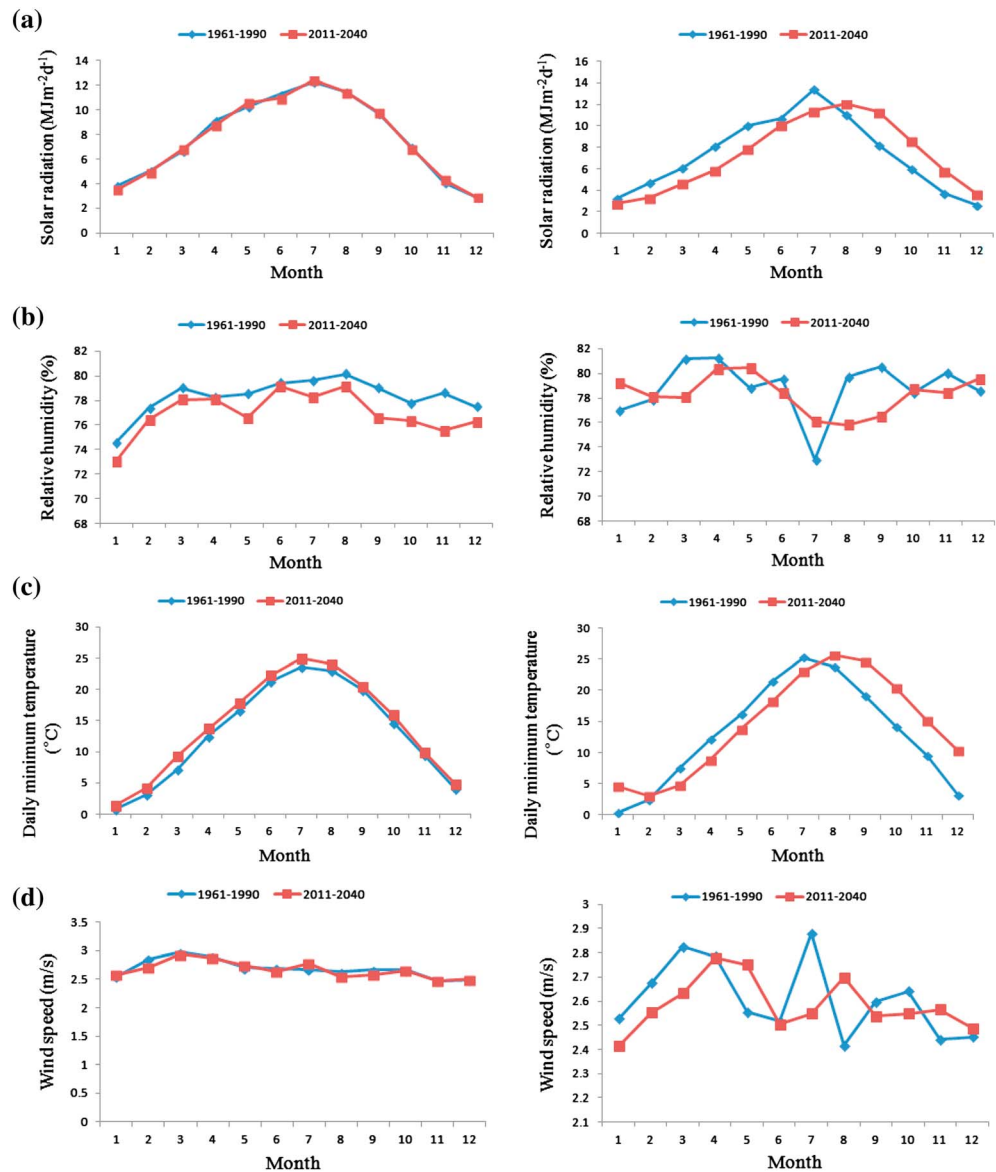


**Figure 13.** Monthly changes in (a) solar radiation, (b) relative humidity, (c) daily minimum temperature, and (d) wind speed in the future period at Hangzhou Station for (left) ECHAM5 and (right) HadCM3.

daily minimum temperature, and wind speed reach +55.5%, +60.0%, and +5.0%, respectively. From the sensitivity analysis results (Figure 3), the relative humidity (29.6%), daily minimum temperature (18.7%), solar radiation (19%), and wind speed (16%) contribute the most to the overall variance of PET according to the first-order effect sensitivity index. PET is also highly sensitive to the interactions between wind speed and relative humidity, whose contribution to the overall PET variance reaches 12%. Such interactions increase the total contribution of wind speed from 16% to 28%. The contribution of relative humidity also increases from 29.6% to 42.9%. It is therefore concluded that in November (winter) the changes in PET are mainly due to the changes in relative humidity, daily minimum temperature, solar radiation, and wind speed (TS = 100%). These four climatic variables all have positive impacts on PET changes, leading to a large increase in PET in November at Hangzhou Station.

Figure 15 shows the changes in solar radiation, relative humidity, daily minimum temperature, and wind speed in the future period at Tianmushan Station for both GCMs. Take September as an example. The PET at Tianmushan Station increases by 45% in this month. Figure 3 shows that in September the increase in solar radiation (20%),

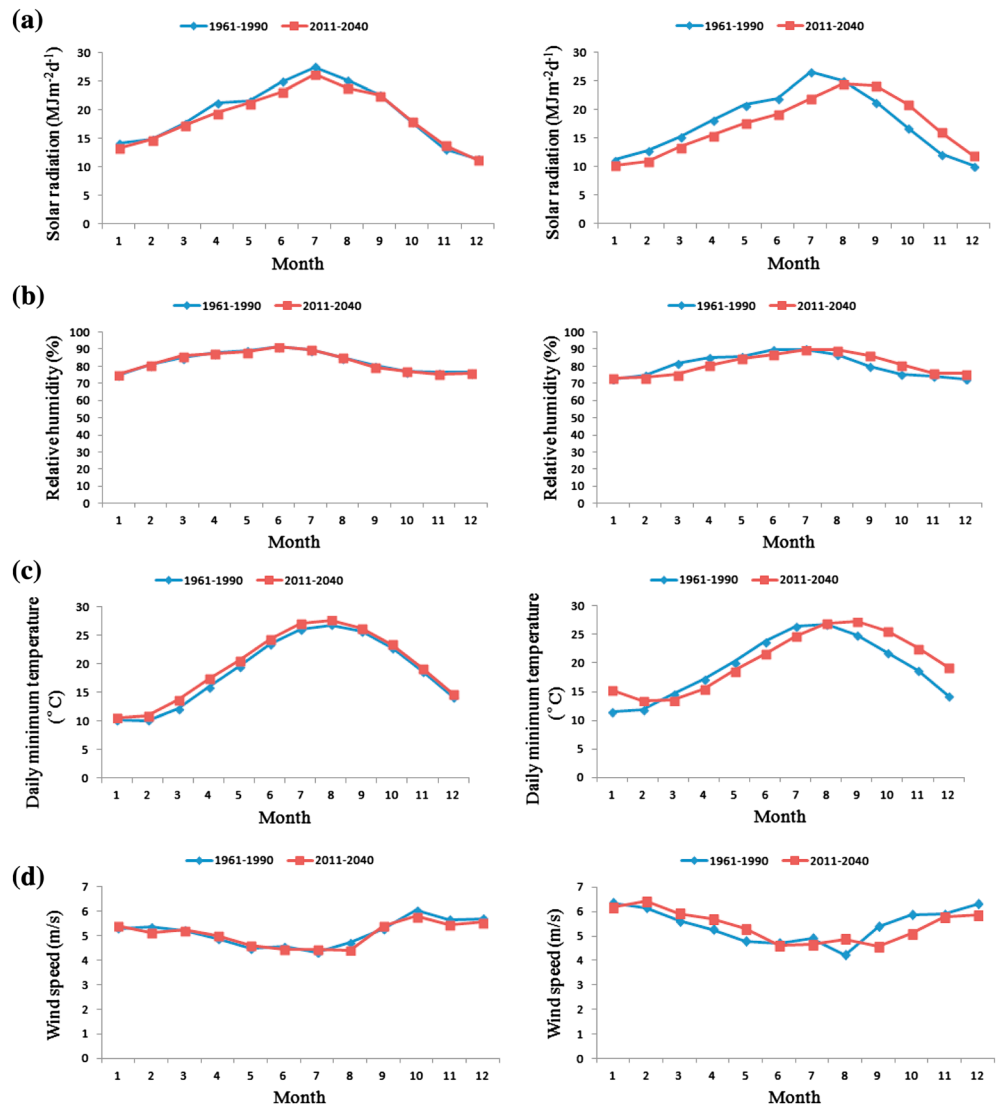


**Figure 14.** Monthly changes in (a) solar radiation, (b) relative humidity, (c) daily minimum temperature, and (d) wind speed in the future period at Dachendao Station for (left) ECHAM5 and (right) HadCM3.

decrease in relative humidity (−3%), and increase in daily minimum temperature (33%) are the major contributions (TS = 93%) to PET changes, and other climatic variables have less important impact (TS < 10%).

The above analysis also applies for Dachendao, although the changes in future PET are less obvious than in the other two stations. The largest increase for HadCM3 occurs in November (winter). Changes in relative humidity, solar radiation, daily minimum temperature, and wind speed in this month are 2.6%, 31%, 21%, and 5.79%, respectively. According to Figure 3, the contributions of relative humidity, solar radiation, daily minimum temperature, and wind speed to the total variance of PET are 78%, 4.2%, 11%, and 14%, respectively. Although the change in relative humidity in the future period is relatively small, the contribution of this climatic variable to PET changes is still substantial due to its high sensitivity to PET in winter. Meanwhile, the role of wind speed cannot be ignored.

The above monthly analysis also indicates the causes of PET changes on an annual or seasonal scale. For example, as stated in section 3.4, the annual mean PET increases for both GCMs in the whole province. It can be figured out that at all three stations, the positive changes in solar radiation and daily minimum temperature contribute substantially to the increases in annual mean PET, while the changes in relative humidity are as important as changes in solar radiation and daily minimum temperature at Dachendao. On a seasonal scale, the role of wind speed cannot be ignored, particularly in winter.

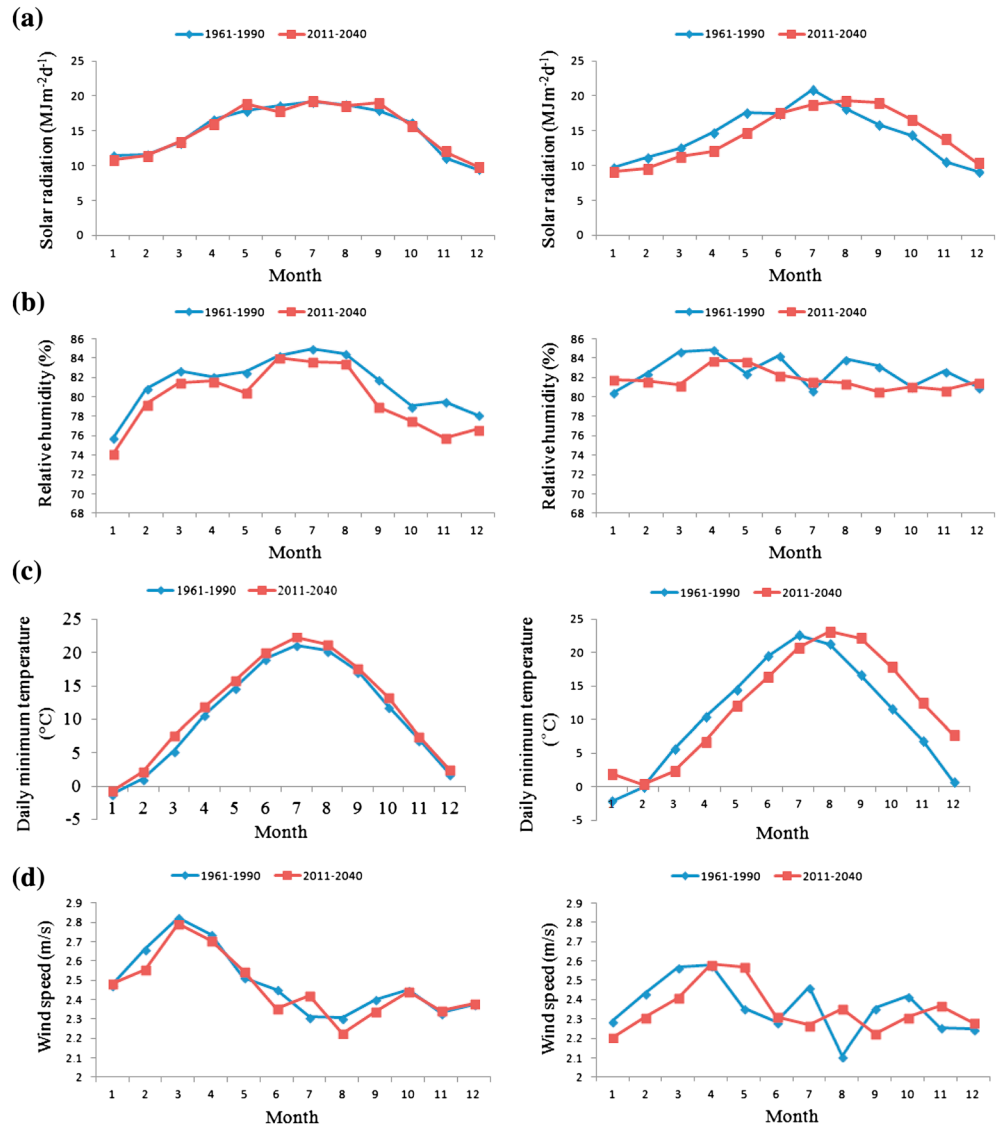


**Figure 15.** Monthly changes in (a) solar radiation, (b) relative humidity, (c) daily minimum temperature, and (d) wind speed in the future period at Tianmushan Station for (left) ECHAM5 and (right) HadCM3.

As mentioned in section 3.4, it can be observed from Figure 12 that HadCM3 projects more substantial monthly changes of PET than ECHAM5 at three stations. This can be explained by larger variations in different monthly climatic variables projected by HadCM3, which are shown in Figures 13–15. In particular, the changes in solar radiation and daily minimum temperatures are substantial.

#### 4. Discussion

It is important to understand why PET has changed in the province and what the main causes are for hydrological modeling and agricultural water management. This study therefore used a global sensitivity analysis method, Sobol's method, to determine the sensitivity of PET to different climatic variables. This method can apportion the output uncertainty to the uncertainty in the input factors and meanwhile take the interactions among variables into account. The results in this paper highlighted the great sensitivity of PET in the study area to solar radiation during the summer period, when PET reaches its highest values. Relative humidity has a much larger impact on PET estimation than other climatic variables in the winter period when PET reaches its lowest values. This confirms the finding from a previous study by Gong *et al.* [2006] that PET is

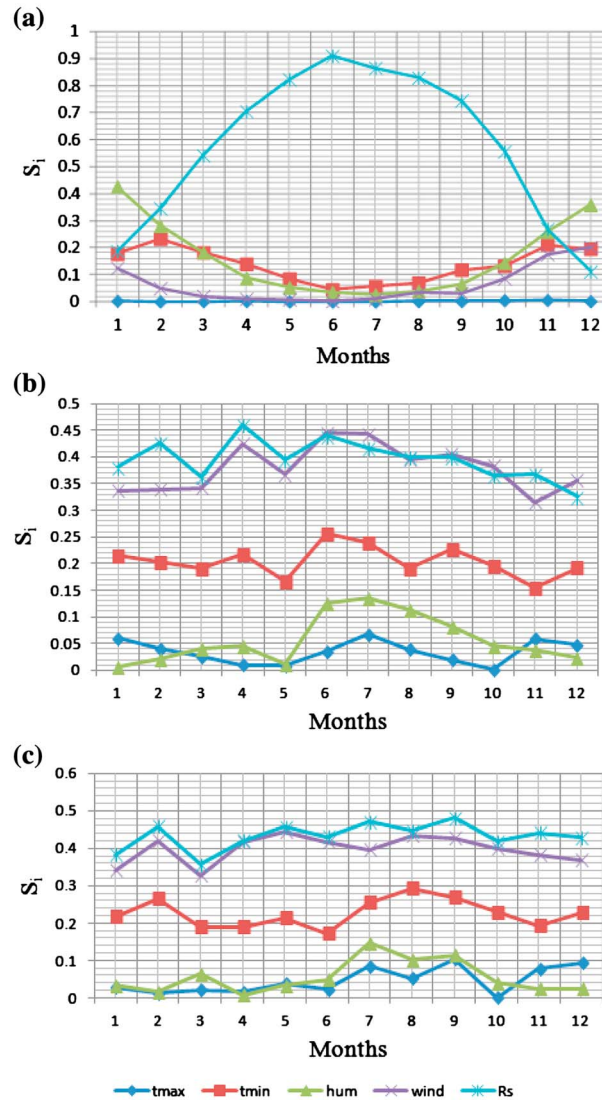


**Figure 16.** First-order effect sensitivity index based on data from (a) the observation, (b) PRECIS-simulated baseline data, and (c) PRECIS-simulated future data at Cunan.

very sensitive to relative humidity or shortwave radiation in the Yangtze River basin using the sensitivity coefficient method. *Thomas* [2000] also concluded that relative humidity is the most important factor at 11 stations in east China by contributing 17% to the variance based on a linear stepwise multivariate regression. Meanwhile, other studies have investigated the sensitivity of pan evaporation, potential evapotranspiration, and actual evapotranspiration to climatic variables as well [Goyal, 2004; Xu et al., 2006; Yang and Yang, 2012]. However, in these studies, the sensitivity has been explored either qualitatively or by first-order approach. Sensitivity analysis results in this study are, in general, consistent with these studies but reveal more detailed information on the spatial-temporal variations in the PET sensitivity and on the interactions between climatic variables. Particularly, the interactions between relative humidity and wind speed, relative humidity, and daily minimum temperature cannot be ignored. As stated in section 3.5, considering the interactions, the total contribution of wind speed to the total PET variance in November increased from 16% to 28% at Hangzhou Station. The contribution of relative humidity increased from 29.6% to 42.9%. This study shows that Sobol's method did provide useful information to help understand the changes and causes of PET changes in the future and is an appropriate global sensitivity analysis in climate change impact analysis.

An important assumption used in this study is that the sensitivities of PET to different climate variables are the same in the observation period and the future period. Such assumption was made due to the consideration that the regional climate model may not be able to simulate the sensitivity properly. Figures 16a–16c show the sensitivity of PET (first-order effect sensitivity index) to different climatic variables based on observation data, PRECIS-simulated data in the baseline period, and PRECIS-simulated data in the future period at Cunan Station. Figure 16b indicates that the sensitivity of PET based on PRECIS-simulated data in the baseline period is very different from that based on observations, indicating that the regional climate model did fail to preserve the sensitivity of PET in the baseline period. The sensitivity in the future period is, however, similar to that in the baseline period. Therefore, the assumption of same sensitivity in the baseline period and future period remains valid when the regional climate model fails to preserve the sensitivity of PET to different climatic variables.

In this study, a Delta change method was used to project the PET in the future period 2011–2040. This is a direct and simple way of avoiding the bias in climatic variables derived from the regional climate model. Although bias correction on precipitation and temperature is often done in the literature [Themeßl et al., 2012; Tian et al., 2013], bias correction on other climatic variables is rarely implemented. It would be better to correct the bias in all variables before they are used to compute PET as long as sophisticated bias correction approaches and enough

observations are available. *Haddeland et al.* [2012] made an investigation on the role of bias correcting climate model radiation, humidity, and wind and found better simulated evapotranspiration and runoff using bias-corrected climate forcing.

Previous studies show that large uncertainty exists in climate change impact analysis, which comes from GCMs, downscaling approaches, emission scenarios, and impact analysis model (here FAO-PM method) [Wilby and Harris, 2006; Kay et al., 2009; Chiew et al., 2010; Xu et al., 2013]. In this study, only one regional climate model with two GCMs and a medium greenhouse gas emission scenario were used to generate future climate change scenarios. Changes in monthly PET for two GCMs already showed substantial differences, indicating large uncertainty in PET projections. Therefore, using limited GCMs and emission scenario will underestimate the uncertainty in future potential evapotranspiration and changes. Although the results in this study are quite helpful to understand future potential evapotranspiration changes, a systematic analysis of uncertainty in future PET projections is proposed to promote the applications of climate change impact analysis in regional water management.

## 5. Conclusions

In this study, the sensitivity of potential evapotranspiration to different climatic variables in Zhejiang Province, East China, was first quantified using a global sensitivity analysis method, Sobol's method. Then future changes of potential evapotranspiration in 2011–2040 were obtained via a regional climate model. The sensitivity analysis results were finally used to analyze the contributions of climatic variable changes to future potential evapotranspiration changes in the province. The key findings of this study are summarized below:

1. Sensitivity analysis results reveal substantial spatial-temporal variations in the sensitivity of PET to climatic variables and unignorable interactions. PET is most sensitive to solar radiations in majority parts of the province, followed by relative humidity, daily minimum temperature, wind speed, and daily maximum temperature. At islands like Dachendao, however, the relative humidity is the most sensitive climatic variable, although in summer solar radiation becomes the dominant variable.
2. In the future period (2011–2040), ECHAM5 projected similar spatial distribution of PET with that in the baseline period (1961–1990), while PET for HadCM3 showed different spatial distribution. For both GCMs, annual mean PET increases in the whole province, although such change might not be significant (<10%). Seasonal or monthly changes are, however, very different. ECHAM5 projected increases in spring, autumn, and winter. Slight decreases are found near the coast in summer. HadCM3 projected decreases in spring and summer, while increases in PET in autumn and winter can be found.
3. On the basis of sensitivity analysis results, the contributions of different climatic variables to PET changes at different months and stations can be revealed. In general, solar radiation, relative humidity, and daily minimum temperature are the three major contributors to PET changes in the future period 2011–2040. However, causes of future PET changes are varied at different stations and months.

## Acknowledgments

We acknowledge the financial support from the International Science & Technology Cooperation Program of China (2010DFA24320) and the National Natural Science Foundation of China (51379183; 50809058). We would also like to thank both the National Climate Center of China Meteorological Administration and Zhejiang Meteorological Administration for providing meteorological data used in this study. The valuable comments and suggestions from the Editor and three anonymous reviewers are greatly appreciated.

## References

- Allen, R. G., M. Smith, A. Perrier, and L. S. Pereira (1994), An update for the calculation of potential evapotranspiration, *ICID Bull.*, *43*, 35–92.
- Blaney, H. F., and W. D. Criddle (1950), Determining water requirements in irrigated areas from climatological irrigation data, *Tech. Pap.* *96*, 48 pp., US Department of Agriculture, Soil Conservation Service, Washington, D. C.
- Chiew, F. H. S., D. G. C. Kirono, D. M. Kent, A. J. Frost, S. P. Charles, B. Timbal, K. C. Nguyen, and G. Fu (2010), Comparison of runoff modeled using rainfall from different downscaling methods for historical and future climates, *J. Hydrol.*, *387*(1–2), 10–23.
- Diodato, N., and G. Bellocchi (2007), Modeling reference evapotranspiration over complex terrains from minimum climatological data, *Water Resour. Res.*, *43*, W05444, doi:10.1029/2006WR005405.
- Donohue, R., T. R. McVicar, and M. L. Roderick (2010), Assessing the ability of potential evaporation formulations to capture the dynamics in evaporative demand within a changing climate, *J. Hydrol.*, *386*, 186–197.
- Fan, Z. X., and A. Thomas (2013), Spatiotemporal variability of reference evapotranspiration and its contributing climatic factors in Yunan Province, SW China, 1961–2004, *Clim. Change*, *116*, 309–325.
- Fowler, H. J., M. Ekström, S. Blenkinsop, and A. P. Smith (2007), Estimating change in extreme European precipitation using a multimodel ensemble, *J. Geophys. Res.*, *112*, D18104, doi:10.1029/2007JD008619.
- Fu, G., Z. Kapelan, and P. Reed (2012), Reducing the complexity of multiobjective water distribution system optimization through global sensitivity analysis, *J. Water Resour. Plann. Manage.*, *138*, 196–207.
- Ge, G., D. Chen, G. Ren, Y. Chen, and Y. Liao (2006), Spatial and temporal variations and controlling factors of potential evapotranspiration in China: 1956–2000, *J. Geogr. Sci.*, *16*(1), 3–12.
- Gong, L., C. Xu, D. Chen, S. Halldin, and Y. D. Chen (2006), Sensitivity of the Penman-Monteith reference evapotranspiration to key climatic variables in the Changjiang (Yangtze River) basin, *J. Hydrol.*, *329*, 620–629.
- Goovaerts, P. (2000), Geostatistical approaches for incorporating elevation into the spatial interpolation of rainfall, *J. Hydrol.*, *228*, 113–129.

- Gordon, C., C. Cooper, A. Senior, H. Banks, J. M. Gregory, T. C. Johns, J. F. B. Mitchell, and R. A. Wood (2000), The simulation of SST, sea ice extents and ocean heat transports in a version of the Hadley Centre coupled model without flux adjustments, *Clim. Dyn.*, *16*, 147–168.
- Goyal, R. K. (2004), Sensitivity of evapotranspiration to global warming: A case study of arid zone of Rajasthan (India), *Agric. Water Manage.*, *69*, 1–11.
- Gu, S., et al. (2008), Characterizing evapotranspiration over a meadow ecosystem on the Qinghai-Tibetan Plateau, *J. Geophys. Res.*, *113*, D08118, doi:10.1029/2007JD009173.
- Haddeland, I., J. Heinke, F. Voß, S. Eisner, C. Chen, S. Hagemann, and F. Ludwig (2012), Effects of climate model radiation, humidity and wind estimates on hydrological simulations, *Hydrol. Earth Syst. Sci.*, *16*, 305–318.
- Hargreaves, G. H., and Z. A. Samni (1982), Estimation of potential evapotranspiration, *J. Irrig. Drain. Div., Proc. Am. Soc. Civ. Eng.*, *108*, 223–230.
- Hargreaves, G. H., and Z. A. Samni (1985), Reference crop evapotranspiration from temperature, *Appl. Eng. Agr.*, *1*(2), 96–99, doi:10.13031/2013.26773.
- Haynes, C. P., and C. Millet (2013), A sensitivity analysis of meteoric infrasound, *J. Geophys. Res. Planets*, *118*, 2073–2082, doi:10.1002/jgre.20116.
- Heo, K. Y., K. J. Ha, K. S. Yun, S. S. Lee, H. J. Kim, and B. Wang (2013), Methods for uncertainty assessment of climate models and model predictions over East Asia, *Int. J. Climatol.*, doi:10.1002/joc.3692.
- Jha, M., Z. Pan, E. S. Takle, and R. Gu (2004), Impacts of climate change on streamflow in the Upper Mississippi River Basin: A regional climate model perspective, *J. Geophys. Res.*, *109*, D09105, doi:10.1029/2003JD003686.
- Jones, R. G., M. Noguer, D. Hassell, D. Hudson, S. Wilson, G. Jenkins, and J. Mitchell (2004), *Generating High Resolution Climate Change Scenarios Using PRECIS*, Hadley Centre for Climate Prediction and Research, pp. 40, Met Office Hadley Centre, U. K.
- Kay, A., H. Davies, V. Bell, and R. Jones (2009), Comparison of uncertainty sources for climate change impacts: Flood frequency in England, *Clim. Change*, *92*(1–2), 41–63.
- Li, X., and Q. Zhang (2011), Estimating the potential evapotranspiration of Poyang Lake Basin using remote sense data and Shuttleworth-Wallace Model, *Procedia Environ. Sci.*, *10*, 1575–1582.
- Li, W., R. E. Dickinson, R. Fu, G. Y. Niu, Z. L. Yang, and J. G. Canadell (2007), Future precipitation changes and their implications for tropical peatlands, *Geophys. Res. Lett.*, *34*, L01403, doi:10.1029/2006GL028364.
- Li, Z., F. Zheng, and W. Z. Liu (2012), Spatiotemporal characteristics of reference evapotranspiration during 1961–2009 and its projected changes during 2011–2099 on the Loess Plateau of China, *Agric. For. Meteorol.*, *154–155*, 147–155.
- Liu, B., M. Xu, M. Henderson, and W. Gong (2004), A spatial analysis of pan evaporation trends in China, 1955–2000, *J. Geophys. Res.*, *109*, D15102, doi:10.1029/2004JD004511.
- Makkink, G. F. (1957), Testing the Penman formula by means of lysimeters, *J. Inst. Water Eng.*, *11*, 277–288.
- McVicar, T. R., T. G. van Niel, L. T. Li, M. F. Hutchinson, X. M. Mu, and Z. H. Liu (2007), Spatially distributing monthly reference evapotranspiration and pan evaporation considering topographic influences, *J. Hydrol.*, *338*, 196–220.
- Onof, C., and K. Arnbjerg-Nielsen (2009), Quantification of anticipated future changes in high resolution design rainfall for urban areas, *Atmos. Res.*, *92*, 350–363.
- Priestley, C. H. B., and R. J. Taylor (1972), On the assessment of surface heat flux and evaporation using large-scale parameters, *Mon. Weather Rev.*, *100*, 81–92.
- Reichler, T., and J. Kim (2008), How well do coupled models simulate today's climate?, *Bull. Am. Meteorol. Soc.*, *1989*, 303–311.
- Roekner, E., et al. (2003), The atmospheric general circulation model ECHAM5. Part I: Model description, Max Planck Institute for Meteorology Rep. 349, 127 pp. [Available from MPI for Meteorology, Bundesstr. 53, 20146 Hamburg, Germany.]
- Rohwer, C. (1931), Evaporation from free water surface, *USDA Tech. Null.*, *217*, 1–96.
- Saltelli, A., and P. Annoni (2010), How to avoid a perfunctory sensitivity analysis, *Environ. Modell. Softw.*, *25*, 1508–1517.
- Saltelli, A., K. Chan, and E. M. Scott (2000), *Sensitivity Analysis*, John Wiley, England.
- Simmons, A. J., D. M. Burridge, M. Jarraud, C. Girard, and W. Wergen (1989), The ECMWF medium-range prediction models development of the numerical formulations and the impact of increased resolution, *Meteorol. Atmos. Phys.*, *40*, 28–60.
- Sobol', I. M. (1993), Sensitivity analysis for non linear mathematical models, *Math. Model. Comput. Exp.*, *1*, 407–414.
- Stott, P. A., S. F. B. Tett, G. S. Jones, M. R. Allen, J. F. B. Mitchell, and G. J. Jenkins (2000), External control of 20th century temperature by natural and anthropogenic forcings, *Science*, *290*, 2133–2137.
- Tang, Y., P. Reed, T. Wagener, and K. van Werkhoven (2007), Comparing sensitivity analysis methods to advance lumped watershed model identification and evaluation, *Hydrol. Earth Syst. Sci.*, *11*, 793–817.
- Thiemeßl, M. J., A. Gobiet, and G. Heinrich (2012), Empirical-statistical downscaling and error correction of regional climate models and its impact on the climate change signal, *Clim. Change*, *112*, 449–468.
- Thomas, A. (2000), Spatial and temporal characteristics of potential evapotranspiration trends over China, *Int. J. Climatol.*, *20*, 381–396.
- Tian, Y., Y. P. Xu, and X. Zhang (2013), Assessment of climate change impacts on river high flows through comparative use of GR4J, HBV and Xinanjiang Models, *Water Resour. Manage.*, *27*(8), 2871–2888.
- Van der Velde, Y., S. W. Lyon, and G. Destouni (2013), Data-driven regionalization of river discharges and emergent land cover-evapotranspiration relationships across Sweden, *J. Geophys. Res. Atmos.*, *118*, 2576–2587, doi:10.1002/jgrd.50224.
- Wang, W., S. Peng, Y. Tao, Q. Shao, J. Xu, and W. Xing (2011), Spatial and temporal characteristics of reference evapotranspiration trends in the Haihe River Basin, China, *J. Hydrol. Eng.*, *16*, 239–252.
- Wang, G. Q., J. Y. Zhang, J. L. Jin, T. C. Pagano, R. Calow, Z. X. Bao, C. S. Liu, Y. L. Liu, and X. L. Yan (2012), Assessing water resources in China using PRECIS projections and a VIC model, *Hydrol. Earth Syst. Sci.*, *16*, 231–240.
- Wang, W., W. Xing, Q. Shao, Z. Yu, S. Peng, T. Yang, B. Yong, J. Taylor, and V. P. Singh (2013), Changes in reference evapotranspiration across the Tibetan Plateau: Observations and future projections based on statistical downscaling, *J. Geophys. Res. Atmos.*, *118*, 4049–4068, doi:10.1002/jgrd.50393.
- Wilby, R. L., and I. Harris (2006), A framework for assessing uncertainties in climate change impacts: Low-flow scenarios for the River Thames, UK, *Water Resour. Res.*, *42*, W02419, doi:10.1029/2005WR004065.
- Woldemeskel, F. M., A. Sharma, B. Sivakumar, R. Mehrotra (2012), An error estimation method for precipitation and temperature projections for future climates, *J. Geophys. Res.*, *117*, D22104, doi:10.1029/2012JD018062.
- Xu, C., L. Gong, T. Jiang, and D. Chen (2006), Analysis of spatial distribution and temporal trend of reference evapotranspiration and pan evaporation in Changjiang (Yangtze River) catchment, *J. Hydrol.*, *327*, 81–93.
- Xu, C., X. Shen, and Y. Xu (2007), An analysis of climate change in East Asia by using the IPCC AR4 simulations, *Adv. Clim. Change Res.*, *3*(5), 287–292.

- Xu, C.-Y., and V. P. Singh (2000), Evaluation and generalization of radiation-based methods for calculating evaporation, *Hydrolog. Process.*, *14*, 339–349.
- Xu, C.-Y., and V. P. Singh (2001), Evaluation and generalization of radiation-based methods for calculating evaporation, *Hydrolog. Process.*, *15*, 305–319.
- Xu, Y., and A. Mynett (2006), Application of uncertainty and sensitivity analysis in river basin management, *Water Sci. Technol.*, *53*(1), 41–49.
- Xu, Y. L., X. Y. Huang, and Y. Zhang (2005), Statistical analyses of climate change scenarios over China in the 21st century, *Adv. Clim. Change Res.*, *1*, 80–83.
- Xu, Y. P., X. Zhang, and Y. Tian (2012), Impact of climate change on 24-h design rainfall depth estimation in Qiantang River Basin, East China, *Hydrolog. Process.*, *26*(26), 4067–4077.
- Xu, Y. P., X. Zhang, Q. Ran, and Y. Tian (2013), Impact of climate change on hydrology of upper reaches of Qiantang River Basin, East China, *J. Hydrol.*, *483*, 51–60.
- Yang, J. (2011), Convergence and uncertainty analyses in Monte-Carlo based sensitivity analysis, *Environ. Modell. Softw.*, *26*, 444–457.
- Yang, H., and D. Yang (2012), Climatic factors influencing changing pan evaporation across China from 1961–2001, *J. Hydrol.*, *414–415*, 184–193.
- Zhang, C., J. Chu, and G. Fu (2013), Sobol's sensitivity analysis for a distributed hydrological model of Yichun River Basin, China, *J. Hydrol.*, *480*, 58–68.
- Zhang, Y., Y. Xu, W. Dong, L. Cao, and M. Sparrow (2006), A future climate scenario of regional changes in extreme climate events over China using the PRECIS climate model, *Geophys. Res. Lett.*, *33*, L24702, doi:10.1029/2006GL027229.
- Zhejiang Provincial Hydrology Bureau (2005), Water resources in Zhejiang Province, Report, Zhejiang, Hangzhou.